



Modeling evolution of the San Andreas Fault system in northern and central California

Anton A. Popov

Section of Geodynamic Modeling, GeoForschungsZentrum, DE-14473 Potsdam, Germany

Now at Institute for Geosciences, Johannes Gutenberg University, DE-55099 Mainz, Germany

Stephan V. Sobolev

Section of Geodynamic Modeling, GeoForschungsZentrum, DE-14473 Potsdam, Germany

Schmidt Institute of Physics of the Earth, 123995 Moscow, Russia

Mark D. Zoback

Department of Geophysics, Stanford University, Stanford, California 94305-2215, USA

[1] We present a three-dimensional finite element thermomechanical model idealizing the complex deformation processes associated with evolution of the San Andreas Fault system (SAFS) in northern and central California over the past 20 Myr. More specifically, we investigate the mechanisms responsible for the eastward (landward) migration of the San Andreas plate boundary over time, a process that has largely determined the evolution and present structure of SAFS. Two possible mechanisms had been previously suggested. One mechanism suggests that the Pacific plate first cools and captures uprising mantle in the slab window, subsequently causing accretion of the continental crustal blocks. An alternative scenario attributes accretion to the capture of plate fragments (microplates) stalled in the ceased Farallon-North America subduction zone. Here we test both these scenarios numerically using a recently developed lithospheric-scale code, SLIM3D, that employs free surface, nonlinear temperature- and stress-dependent elastoviscoplastic rheology and allows for self-generation of faults. Modeling suggests that microplate capture is the primary driving mechanism for the eastward migration of the plate boundary, while the slab window cooling mechanism alone is incapable of explaining this phenomenon. We also show that the system evolves to the present day structure of SAFS only if the coefficient of friction at mature faults is low (0.08 for the best fit model). Thus, our model provides an independent constraint supporting the “weak fault in a strong crust” hypothesis for SAFS.

Components: 10,700 words, 12 figures, 1 table.

Keywords: San Andreas Fault; friction; geodynamics; numeric model; weak fault in strong crust.

Index Terms: 8111 Tectonophysics: Continental tectonics: strike-slip and transform; 8118 Tectonophysics: Dynamics and mechanics of faulting (8004); 8120 Tectonophysics: Dynamics of lithosphere and mantle: general (1213).

Received 2 February 2012; **Revised** 1 May 2012; **Accepted** 27 June 2012; **Published** 25 August 2012.

Popov, A. A., S. V. Sobolev, and M. D. Zoback (2012), Modeling evolution of the San Andreas Fault system in northern and central California, *Geochem. Geophys. Geosyst.*, 13, Q08016, doi:10.1029/2012GC004086.

1. Introduction

[2] The San Andreas Fault System (SAFS) is a complex network of predominantly strike-slip faults that forms a present day boundary between the North American and Pacific plates. The system extends from the Mendocino triple junction (MTJ) on the north to the Gulf of California on the south. SAFS is characterized by a relatively complex tectonics. In particular it is influenced by subduction of the Gorda plate to the north of MTJ, and by a large transpressive bend near the Frazier Park in Southern California, the so-called “big bend”. The present day tectonic regime of the San Andreas plate boundary is essentially transform, with the fault-normal motion being almost an order of magnitude smaller than the fault-parallel [Argus and Gordon, 2001].

[3] The strike-slip deformation is not concentrated on a single fault, but rather partitioned among numerous simultaneously active subparallel faults throughout the California western margin. For example at the latitude of San Francisco, the entire relative velocity is accommodated by Hayward, Calaveras, San Andreas (SAF), and San Gregorio faults [Prescott et al., 2001] (Figure 1). Interpretation of geologic mapping indicates also a significant Neogene slip on the offshore faults, such as the San Gregorio-Hosgri fault zone [Dickinson et al., 2005]. However, the present day Pacific-North America plate boundary is located mostly in the continent, rather than offshore. There is a complex pattern of crustal terrains bounded by faults, which are completely or partially kinematically coupled to the Pacific plate [Argus and Gordon, 2001; Becker et al., 2005]. This fact suggests that there is an eastward migration trend of the principal locus of transform deformation. Landward propagation of the plate boundary occurs in a form of terrain accretion by the Pacific plate, accompanied with a discrete “jump” of the major fault in the system [Dickinson, 1981, 1997]. At least two conceptual models have been proposed in the literature to explain the physical mechanisms responsible for the terrain accretion, that are described below.

1.1. Slab Window Cooling and Microplate Capture

[4] Tectonic reconstructions [Atwater and Stock, 1998; Wilson et al., 2005] have shown that SAFS originated about 27 Ma in response to collision of the East Pacific Rise with the former Farallon-North America subduction zone. The collision

process was accompanied by fragmentation the Farallon plate into several microplates, including the Monterey (27–19 Ma), Arguello (20–18 Ma), Guadalupe (20–14 Ma), Magdalena (14–12 Ma) and Riviera plates (5 Ma–present) [Lonsdale, 1991; Stock and Lee, 1994]. The evolution of SAFS can be explained as a series of the microplate capture events [Nicholson et al., 1994]. Details of the microplate capture process can be briefly summarized as follows. The positive buoyancy of a young partially subducted microplate leads to its detachment from the downgoing slab. The detachment causes cessation of subduction as well as the seafloor spreading. In just a few Myr the microplate becomes effectively coupled to the Pacific plate due to conductive cooling of the ceased ridge segment [Bohannon and Parsons, 1995]. Simultaneously, the rapidly strengthening extinct subduction interface exerts tractions on the overriding plate. Thus, the microplate capture model, also known as the “stalled slab” concept [Bohannon and Parsons, 1995], provides a direct and effective mechanism for transferring of the North American continental crust to the Pacific plate.

[5] Alternatively, the evolution of SAFS can be viewed in the context of the migrating triple junction paradigm [Atwater, 1970; Atwater and Molnar, 1973; Ingersoll, 1982; Severinghaus and Atwater, 1990]. The contact between the Pacific and North America plates lengthens as the Mendocino triple junction (northern end) and Rivera triple junction (southern end) migrate in the opposite directions along the coastline (Figure 1). It was proposed that a slab-free zone or slab window (slab gap) developed beneath North America following its contact with the Pacific plate [Dickinson and Snyder, 1979; Zandt and Furlong, 1982; Furlong et al., 1989; Severinghaus and Atwater, 1990]. Main stages of the slab window formation can be explained as shown in the Figure 2. As opposed to the microplate capture model, the process begins with the subduction of the mid-ocean ridge segment. The spreading terminates at a relatively shallow depth, and the slab south of the triple junction detaches and sinks in the mantle. As the slab north of the triple junction continues to subduct and move northward with respect to the overriding plate, the slab window progressively grows in size and fills with the hot material upwelling from asthenosphere.

[6] Existence of the slab window beneath the northern Coast Ranges is widely supported by geophysical observations. Among those are: the surface uplift pattern [Furlong and Schwartz, 2004],

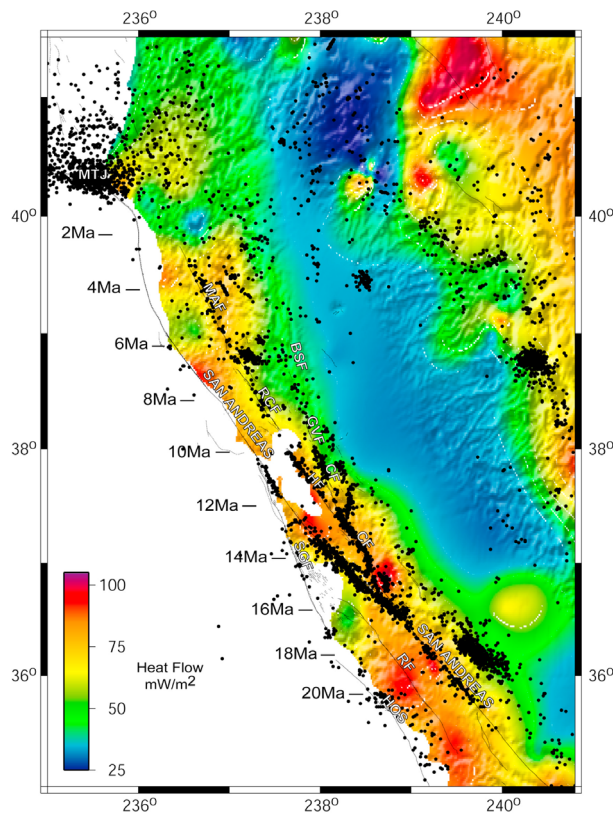


Figure 1. Map illustrating major features of the SAFS in central and northern California. Background colors represent surface heat flow observations from the USGS database. Also shown are the distribution of the seismicity over the past decade (northern California Data Center), topography, and major faults. The numbers to the left side of the San Andreas Fault (shown in red) indicate the positions of the Mendocino triple junction (MTJ) relative to the Great Valley block [Atwater and Stock, 1998]. Other faults shown are the Maacama (MAF), Bartlett Springs (BSF), Rogers Creek (RCF), Green Valley (GVF), Calaveras (CF), Hayward (HF), San Gregorio (SGF), Hosgri (HOS), and Rinconada (RF).

relatively high heat flow values [Lachenbruch and Sass, 1980] (Figure 1), replacement of arc volcanism north of the MTJ with the slab window–related volcanism south of the MTJ [Wilson et al., 2005], thickening and thinning of the North American crust related to the MTJ passage [Beaudoin et al., 1996; Furlong and Govers, 1999]. The large volumes of the low-velocity upper mantle imaged beneath the western U.S. are essentially coincident with the inferred present day location of the slab window [Humphreys and Dueker, 1994].

[7] Accretion of the North American crust to the Pacific plate can be explained in the context of conductive cooling of the uprising asthenospheric material [Furlong, 1984; Furlong et al., 1989;

Furlong, 1993]. Initial temperature distribution in the slab window is unstable due to presence of the lateral temperature gradients. Aging of the slab window and equilibration of the gradients south of the MTJ should cause eastward migration of the locus of maximum mantle temperature. Since the rheology of the rocks is temperature dependent, the mantle shear zone should also migrate eastward, causing accretion of asthenosphere to the Pacific plate. Eventually, when the offset between the crustal and mantle plate boundaries reaches critical value, the crustal fault displaces in the discrete manner (“jumps”) to the east, causing full or partial accretion of the crustal terrain [Furlong et al., 1989]. The upper mantle tomographic images support the slab window cooling model. Benz et al. [1992] detected the southward tapering of the low-velocity zone beneath the Coast Ranges south of the MTJ. This observation can be used as an evidence of the asthenosphere cooling and accretion.

[8] The slab window cooling appears to be the most natural mechanism controlling the terrain accretion processes in central and especially in northern California, as the closest areas to the MTJ. However, it is still unclear whether the influence of the captured microplates can be completely ignored for this region. Previous models, being either two dimensional [Furlong, 1993], or purely thermal [van Wijk et al., 2001], could not consider this problem. van Wijk et al. [2001] studied both the stalled slab and the slab window scenarios for the postsubduction history of Monterey and Arguello microplates. It was, however, impossible to discriminate the scenarios based solely on the thermal constraints. Groome and Thorkelson [2009] calculated the influence of a generic slab window migration and the asthenosphere upwelling on the overriding plate deformation. Their simplified three-dimensional model did not include thermomechanical coupling, which is important in the context of a long-term (>1 Myr) deformation of the lithosphere. Recently Burkett and Billen [2009] performed a two-dimensional simulation of the ridge-trench collision. Dynamics of the slab detachment is a key factor controlling the preference between the slab window and stalled slab scenarios. In this work we consider the consequences of these scenarios for the overriding plate deformation.

[9] To do so we have conducted a series of finite element simulations with the complete thermo-mechanical coupling and the elastoviscoplastic temperature- and stress-dependent rock rheology. The models permit deformation of the free surface,

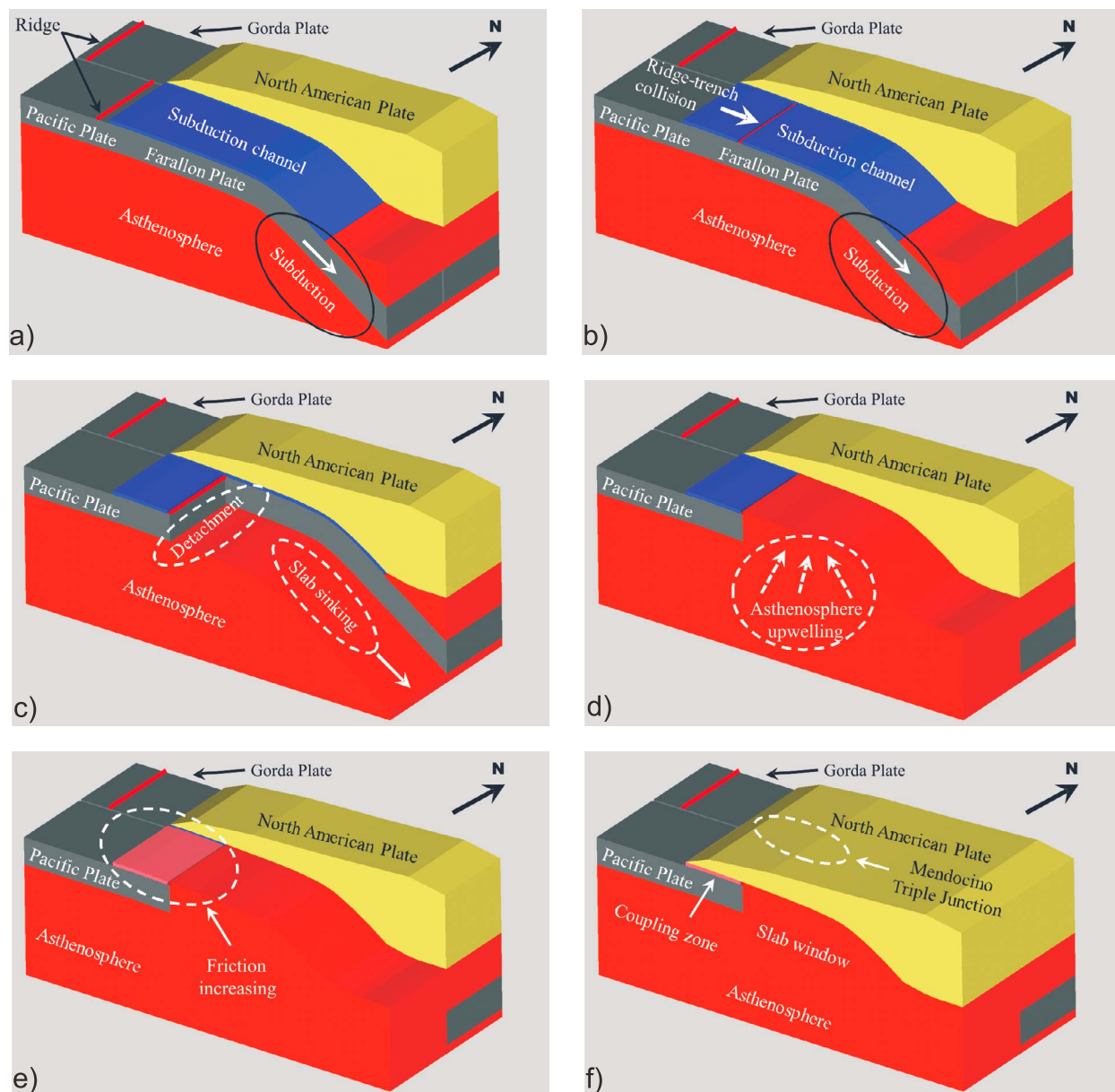


Figure 2. Three-dimensional cartoon illustrating the stages of the slab window formation. (a) Plate tectonic setting just before the ridge-trench collision. Portion of the North American lithosphere removed and underlying subduction channel material is shown. (b) As the subduction continues, the ridge-trench collision occurs. (c) At certain depth the spreading terminates, the portion of the slab detaches along the zone of minimal strength, and sinks in the mantle driven by the slab pull. (d) Hot asthenospheric material upraises and fills the gap coming in contact with thin lithosphere. (e) Termination of the subduction leads to an increase of the coupling in the extinct subduction interface due to fluid escape and healing processes. This in turn causes the capture of the westernmost North American crust by the Pacific plate. (f) Formation of the slab window finishes. As the MTJ migrates northward, the larger pieces of North American crust become accreted to the Pacific.

resolve large strains, and allow for the dynamic generation of the faults [Popov and Sobolev, 2008]. Unlike previous extended 2-D models of transform faults, SAFS [Chéry et al., 2001] and Dead Sea Transform [Sobolev et al., 2005], our model is fully

three dimensional, and in this respect it is similar to the recent model of the oceanic transform faults [Gerya, 2010] and smaller-scale models of the pull-apart basins [Petrinin and Sobolev, 2006, 2008]. Based on the modeling results we investigate the

influence of the idealized Gorda plate subduction and slab window cooling, together with the captured Monterey microplate, on the terrain accretion processes in northern and central California during the last ~20 Myr.

[10] As we will see from the modeling results, frictional strength at mature faults plays a crucial role for the long-term evolution of SAFS. That naturally links our modeling with another issue intensively debated in respect to SAFS, i.e., the frictional strength of SAF and other major faults of SAFS.

1.2. Effective Strength of the Faults

[11] According to the borehole stress measurements [Zoback and Healy, 1992] and the laboratory data [Byerlee, 1978], the effective friction coefficient of the intact crystalline crust is constrained within the range 0.6–0.8. However, there is no general consensus in the literature about the frictional strength of the plate bounding faults, such as the SAF. Some authors [Zoback, 2000] suggest that the fault should be significantly weaker (i.e., smaller friction), than the surrounding crust; others [Scholz, 2000a, 2000b] propose that both fault and crust should be equally strong. The major arguments used by both assumptions are the surface heat flow values (heat flow constraint), and the maximum horizontal stress (SHmax) [Zoback, 2007] orientation (directional constraint).

[12] The absence of the friction contrast between the strong fault and the crust should imply a localized heat flow anomaly above the fault [Lachenbruch and Sass, 1992]. The observations, however, indicate a lack of a narrow fault-related structure in the surface heat flow pattern (Figure 1). Such a contradiction between the observations and the strong fault assumption is referred to as “heat flow paradox” [Lachenbruch and Sass, 1988]. This issue can be principally resolved by the increased advective heat transport. However, it was reported that there is a lack of intensive hydrothermal activity in the region; the heat transfer regime is predominately conductive [Lachenbruch and Sass, 1992].

[13] Alternatively, if the fault is assumed to be weak, the lower stress magnitudes should be expected in the vicinity of the fault, as well as nearly fault-normal orientation of SHmax. The heat flow paradox becomes naturally resolved due to much smaller heat production compared to the high friction model. The borehole stress measurements [Zoback et al., 1987; Hickman and Zoback, 2004], the focal mechanism inversions [Townend and

Zoback, 2001], and the comparison of different sources from the World Stress Map Database [Fuchs and Müller, 2001] indicate a high angle (60–80°) between the SHmax and the San Andreas in central and southern California. Based on the directional constraint, it was concluded that the frictional resistance to slip of the SAF should be low in both absolute and relative senses [Townend and Zoback, 2004].

[14] Even without providing the physical mechanism for the low friction coefficient, the numerical simulations independently support the weak fault hypothesis [Liu and Bird, 2002; Liu et al., 2007; Humphreys and Coblenz, 2007; Carena and Moder, 2009]. A typical model varies the effective friction as a parameter, and considers the fault system solely from the viewpoint of the mechanical equilibrium. With this approach Bird and Kong [1994] constrained the friction coefficient of the SAF to be as low as 0.12, which is much less than a normal value (0.6–0.8). They indicate that in order to reproduce closely the observed slip rates, the fault friction should be made dependent on the accumulated slip. Existence of the slip dependence is also inferred by the directional constraint. Using the stress orientations from the earthquake focal plane mechanisms Provost and Houston [2003] suggested that the SAF is mechanically stronger in the northern part compared to the creeping section in central California; i.e., the strength degrades with the increasing slip and age of the fault.

[15] Recently Li et al. [2009] and Liu et al. [2010] have developed 3-D viscoelastoplastic finite element models to investigate evolution and strain partitioning of SAFS. They discussed the relationship between the fault slips (even on the nonplanar faults) [Li et al., 2009], fault strength and viscosity beneath the fault. These studies also support the weak fault hypothesis, and consider larger spatial extents compared to our work (e.g., eastern California shear zone is included) [Liu et al., 2010]. However, they use predefined faults and model considerably smaller time scales than in this study (at most 100 kyr) [Liu et al., 2010].

[16] Chéry et al. [2001] developed a 3-D finite element model of the strike-slip deformation of the crust with embedded weak zone (the SAF). They considered a relatively short term process (50 kyr) and ignored the along-strike variation of entire fields, as well as the thermomechanical feedback. Even with these assumptions they clearly demonstrated that relative weakness of the fault zone is required, otherwise the slip “leaks” from the fault and

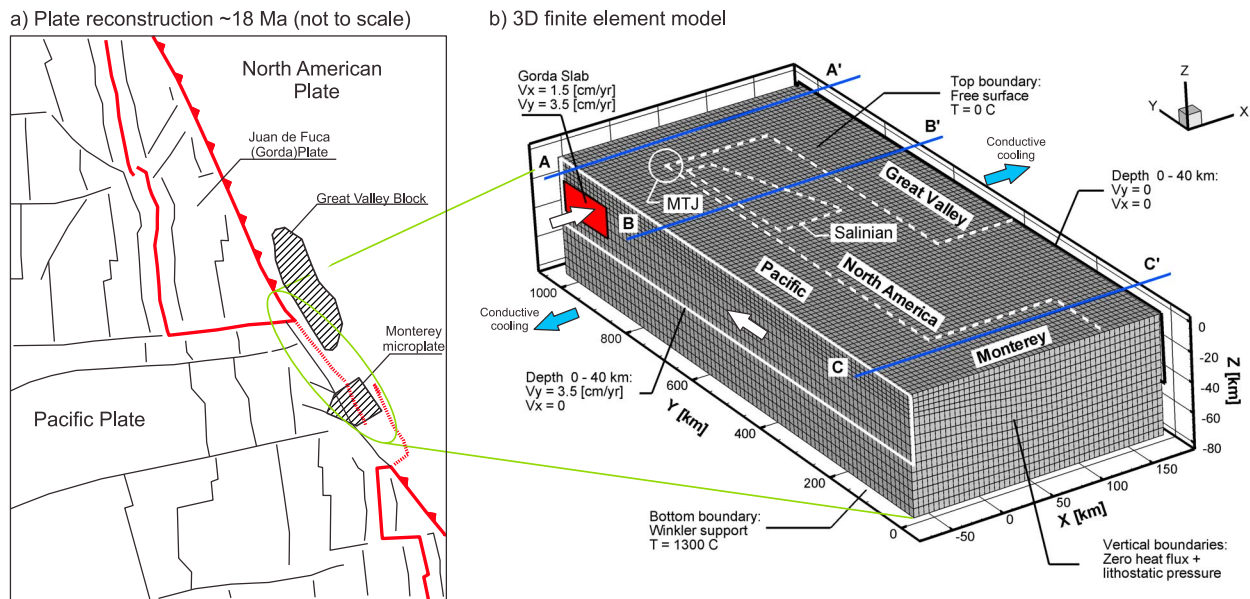


Figure 3. Setup of the three-dimensional model. (a) Approximate positioning of the model domain with respect to the reconstructed plate configuration at about 18 Ma [Atwater and Stock, 1998]. Shown are the tectonic elements included in the model (Gorda plate, Great Valley block, and Monterey microplate). (b) Finite element discretization and boundary conditions of the three-dimensional model. White dashed lines show surface traces of the tectonic elements. White arrows indicate applied plate velocities. Velocities are given in the fixed Great Valley reference frame. Blue arrows indicate nonzero conductive heat flux on the corresponding vertical boundaries. Profiles A-A'–C-C' are shown in Figure 4.

accommodates in the adjacent crust. Quantitatively, the stronger the fault, the more slip leaks. They also showed that the slip can be localized by starting with quite strong fault and introducing strain softening, which is equivalent to the slip weakening in the model. Nevertheless, the weakness of the mature fault (with significant slip) is a necessary prerequisite.

[17] Here we extend the results of Chéry *et al.* [2001] from the viewpoint of the long-term (>1 Myr) 3-D simulation with the complete thermomechanical coupling.

2. Model Setup

[18] The long-term models presented in this paper are based on the tectonic reconstructions of the Pacific-North American plate boundary evolution [Atwater and Stock, 1998; Wilson *et al.*, 2005]. The approximate position and orientation of the model domain with respect to the reconstructed plate configuration is shown in Figure 3a. The modeling time starts at about 18 Ma, shortly after the completion of the Monterey microplate capture [Nicholson *et al.*, 1994]. We consider the interaction between the major tectonic elements in the

region: Pacific plate, Great Valley block, Monterey microplate (Figure 3b). These tectonic elements are represented essentially as the thermal heterogeneities in the mantle. To reproduce the character of the material flow in the asthenosphere upwelling zone, the models also include a simplified subducting Juan de Fuca (presently Gorda) slab. The distance between the idealized Monterey microplate and MTJ is assumed to be 700 km, which is constrained by the Pacific-North America plate boundary length at about 18 Ma [Atwater and Stock, 1998].

[19] Two substantially different model scenarios are considered in this paper. The first scenario aims at studying the thermal equilibration in the slab window alone [Furlong *et al.*, 1989]. In this scenario we assume a two-dimensional initial structure of the slab window to the south of MTJ, and ignore the presence of microplate. The second family of models studies the combined action of the slab window cooling together with the captured Monterey microplate. To match to the first order the observed terrain pattern, and the accumulated slip on the major faults in northern and central California, we argue that the existence of a crustal heterogeneity is required. Figures 3b and 4b show

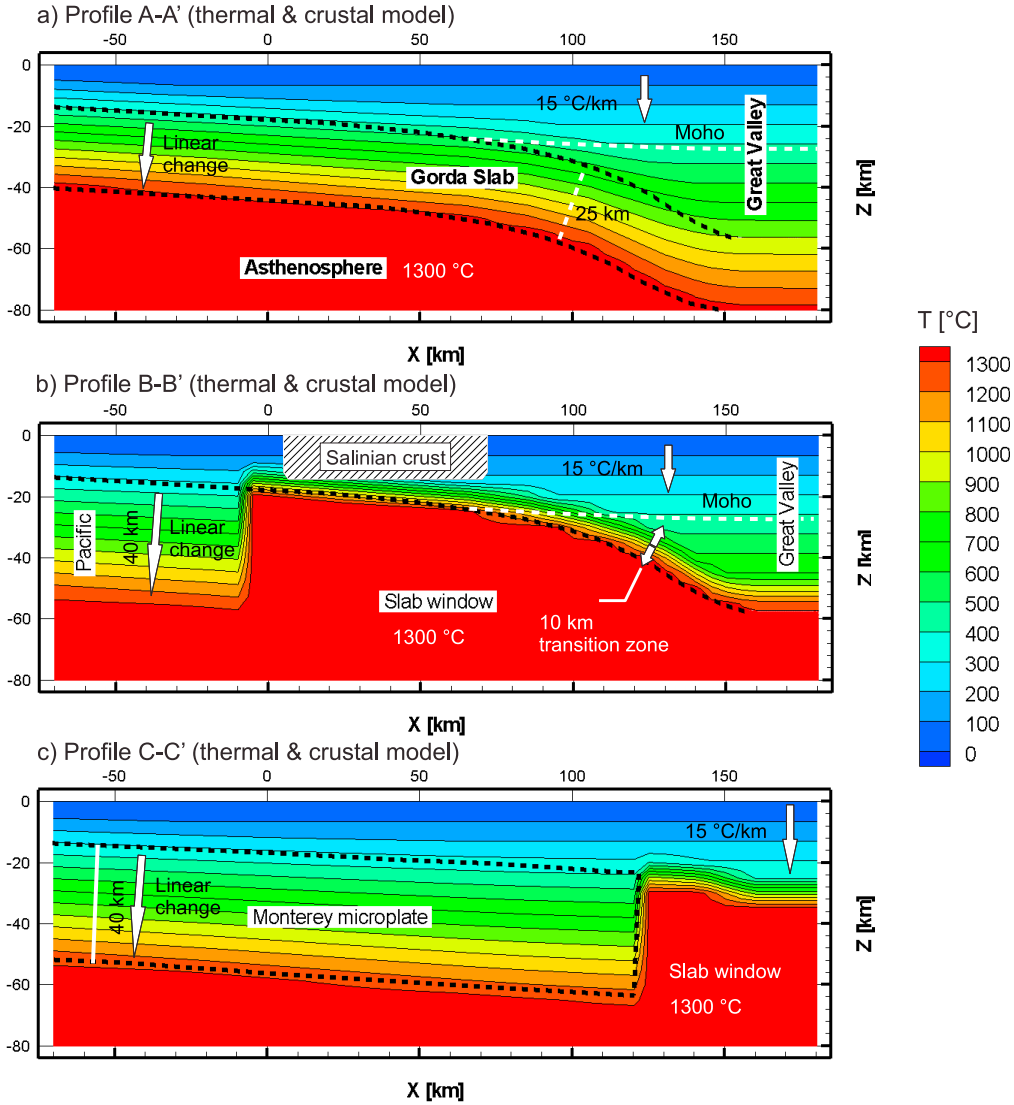


Figure 4. Initial simplified thermal and crustal structure of the model. Colors indicate temperature magnitudes in °C. The uniform initial temperature gradient 15°C/km is assumed. Temperature distribution in the oceanic slabs is linear along the slab thickness. The 10 km transition zone is imposed between the top of the Gorda slab and the slab window. (a) Temperature profile in the Gorda slab (profile A-A'). (b) Initial temperature distribution in the slab window (profile B-B'). (c) Temperature profile in the Monterey microplate (profile C-C'). Positions of the profiles are given in Figure 3. White dashed lines show Moho discontinuity. Hatched area represents Salinian block.

such a heterogeneity, which we interpret as a Salinian block [Irwin, 1990].

2.1. Modeling Approach

[20] We use the thermomechanical finite element modeling tool SLIM3D [Popov and Sobolev, 2008] to solve a coupled system of conservation equations for momentum,

$$\frac{\partial \sigma_{ij}}{\partial x_j} + \rho g_i = 0, \quad (1)$$

and thermal energy,

$$\rho C_p \frac{DT}{Dt} = \frac{\partial}{\partial x_i} \left(\lambda \frac{\partial T}{\partial x_i} \right) + \chi \tau_{ij} (\dot{\epsilon}_{ij}^{vs} + \dot{\epsilon}_{ij}^{pl}) + \rho A. \quad (2)$$

Here x_i ($i = 1, 2, 3$) denote Cartesian coordinates; σ_{ij} is the Cauchy stress tensor; ρ is the material density; g_i is the gravity acceleration vector; C_p is the specific heat; λ is the thermal conductivity; T is the temperature; $0 \leq \chi \leq 1$ is the parameter regulating degree of the thermomechanical feedback; τ_{ij} is the stress deviator; $\dot{\epsilon}_{ij}^{vs}$ and $\dot{\epsilon}_{ij}^{pl}$ are the viscous and

plastic components of the strain rate deviator, respectively; D/Dt stands for the material time derivative; and A is the radiogenic heat production.

[21] Constitutive equations used in SLIM3D are highly nonlinear and include the effects of elastic compressibility and thermal expansion for the pressure,

$$\frac{Dp}{Dt} = -K \left(\dot{\theta} - \alpha \frac{DT}{Dt} \right), \quad (3)$$

and elastoviscoplasticity for the deviatoric stresses,

$$\dot{\epsilon}_{ij} = \dot{\epsilon}_{ij}^{el} + \dot{\epsilon}_{ij}^{vs} + \dot{\epsilon}_{ij}^{pl} = \frac{1}{2G} \hat{\tau}_{ij} + \frac{1}{2\eta_{eff}} \tau_{ij} + \dot{\gamma} \frac{\partial Q}{\partial \tau_{ij}}. \quad (4)$$

Here K and G denote bulk and shear elastic moduli, respectively; p is the pressure; $\dot{\theta}$ is the volumetric strain rate; α is thermal expansion coefficient; $\dot{\epsilon}_{ij}^{el}$ is the elastic component of the strain rate deviator; $\hat{\tau}_{ij}$ is the objective rate of the stress deviator; η_{eff} is the effective creep viscosity; $\dot{\gamma}$ is the plastic multiplier; and Q is the plastic potential function [Simo and Hughes, 2000]. In this work we only include the effect of Dislocation creep [Kameyama et al., 1999]. In this case the expression for the effective viscosity can be written in the following form:

$$\eta_{eff} = \frac{\tau_{II}}{2\dot{\epsilon}_N}, \quad (5)$$

where τ_{II} is the second invariant of stress deviator and $\dot{\epsilon}_N$ is the effective strain rate of the dislocation creep, given by

$$\dot{\epsilon}_N = B_N (\tau_{II})^n \exp\left(-\frac{H_N}{RT}\right). \quad (6)$$

Here B_N , n , and H_N denote, respectively, pre-exponential constant, stress exponent, and activation enthalpy of the Dislocation creep and $R \approx 8.31[J/mol/K]$ is the universal gas constant. Brittle deformation is described by the Mohr-Coulomb plasticity model, with the yield surface written as

$$F = \frac{1}{2}(\sigma_{\max} - \sigma_{\min}) + \frac{1}{2}(\sigma_{\max} + \sigma_{\min})\sin\phi - c \cos\phi, \quad (7)$$

where σ_{\min} and σ_{\max} are the minimum and maximum principal stresses, respectively; ϕ is the internal friction angle; and c is the cohesion. To facilitate comparison of our results with the other works, we use here the friction coefficient (μ) instead of the friction angle (ϕ). The magnitudes of the friction coefficient are uniquely converted to the Mohr-Coulomb friction angles for internal

use in the code, as given, e.g., by Zienkiewicz and Taylor [2000].

[22] The conservation equations are discretized in space using the trilinear constant stress hexahedral finite elements, and in time using the unconditionally stable Backward-Euler algorithm. The discretized physically and kinematically nonlinear system is linearized using the Newton–Raphson iterative scheme, and solved in terms of the incremental displacements (velocity), and temperature primitive variables. We use particle in cell approach [Harlow and Welch, 1965] coupled with the Arbitrary Lagrangian-Eulerian kinematic formulation to resolve the material advection together with the free surface deformation. We refer to Popov and Sobolev [2008] for more details regarding the formulation and implementation of computation procedures used in SLIM3D.

2.2. Strain Localization

[23] Strictly speaking, we do not treat faults here as internal discontinuities, because we are using continuum approach. However, the faults in our models can be associated with the narrow zones of localized strain. The nonlinear rheology employed in SLIM3D is capable of producing such strain localization. In more detail, the sources of strain localization include (1) nonlinear stress dependence in the creep law (equation (6)) (stress increase causes viscosity decrease), (2) thermomechanical feedback (equations (2) and (6)) (temperature increase due to viscous and plastic deformation causes viscosity decrease), and (3) plasticity model with strain softening.

[24] The strain softening model is a simple parameterization of the strength reduction due to elevated fluid pressure [Faulkner and Rutter, 2001], and intrinsically low friction coefficients of the clay minerals forming in the fault gouge [Morrow et al., 2000]. The physical friction is replaced with an effective friction, which is made dependent on the accumulated plastic strain, defined as

$$\kappa = \int_t \sqrt{\dot{\epsilon}_{ij}^{pl} \dot{\epsilon}_{ij}^{pl}} dt. \quad (8)$$

We assume a linear reduction of the effective friction coefficient between the initial value (μ_0) and the saturated value ($\mu_{saturated}$), on the κ interval $[0, \kappa_{critical}]$ (Figure 5). In all the models shown here μ_0 remains the same, and $\mu_{saturated}$ is varied as a free model parameter used to better fit the observations. The strain softening acts as localizing factor, because the friction coefficient reduces with the

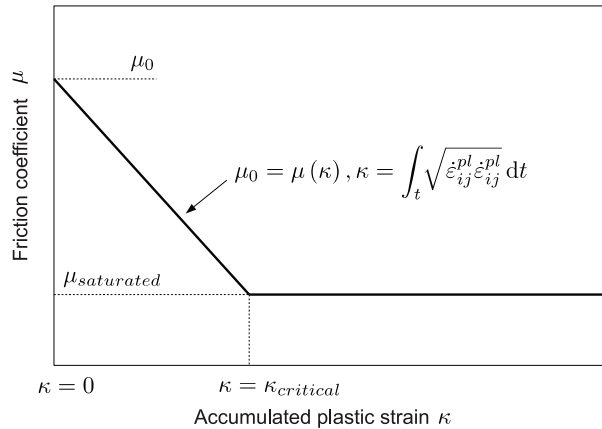


Figure 5. Dependence of the effective friction coefficient (μ) on the accumulated plastic strain (κ).

plastic strain (fault slip) increase, making the incipient fault relatively weaker than the surrounding crust. Hence, weaker zone attract more deformation. Form this viewpoint, the faults in our models are not prescribed (because we start with the same friction coefficient everywhere), but rather self-generated as a result of strain localization. In the context of the long-term deformation considered in this work, the effect of strain rate weakening can be ignored as relatively less important compared to strain softening.

2.3. Discretization and Boundary Conditions

[25] The model domain spans laterally 250 by 1100 km, and 80 km in depth. Figure 3b shows the finite element discretization containing ~ 70000 elements. The entire plate velocities used in the model are calculated with respect to the fixed Great Valley reference frame. We use the reference frame of the Mendocino triple junction to fix the model box. Material can enter and leave the box through the northwestern and southeastern boundaries, and from below.

[26] We assume a constant Pacific plate velocity 3.5 cm/yr [Argus and Gordon, 2001] throughout the modeling time. The y axis of the model coordinate system is assigned to be coincident with the direction of the Pacific plate velocity. The convergent velocity component between the Pacific and Great Valley is small at present (< 3 mm/yr) [Argus and Gordon, 2001], therefore it is assumed to be zero. Substantial change of the Pacific plate direction about 8 Ma [Atwater and Stock, 1998] is also ignored. It is supposed that Juan de Fuca (Gorda)

plate moved northwestward in accord with Pacific plate (3.5 cm/yr), and converged toward the North America with the velocity 1.5 cm/yr (perpendicular direction) (Figure 3b). Velocities in the entire grid points that belong to the Gorda slab are prescribed. The kinematical conditions are applied to both the Pacific plate and the Great Valley on the western and eastern boundaries of the domain above the 40 km depth (Figure 3b). Below this level and on the other vertical boundaries we impose lithostatic pressure. The top boundary of the domain is assumed to be the free surface. On the bottom boundary the Winkler condition is enforced, which implies zero tangential traction, and pressure proportional to the vertical motions of the boundary.

[27] To adequately represent the interaction of the Gorda slab with the overriding North America plate, a weak subduction channel is implemented in our models. We specify a 5 km thick zone above the top boundary of the idealized slab, and assign low friction coefficient (~ 0.05) [Sobolev and Babeyko, 2005] to all material particles that reside in this zone. Resulting friction field is interpolated to the finite element mesh together with the other material parameters.

[28] The formulation of the thermal boundary condition includes prescribed temperatures on the top and bottom boundaries: 0 and 1300°C, respectively, and zero heat flow on the northwestern and southeastern boundaries. To include the influence of heat exchange with surrounding tectonic elements, the thermal equations are solved on a domain which extends 100 km further than model domain to the west and east. This implies a nonzero heat fluxes through the correspondent vertical boundaries, and adequately represents the interaction of the hot uprising material with the cold neighboring Pacific plate and Great Valley mantle.

2.4. Thermal and Crustal Models

[29] Initial temperature distribution remains largely uncertain due to a lack of sufficient paleoconstraints. We adopt a simplified approach here. The three-dimensional initial temperature distribution is shown in Figure 4. Both the geometry of the Gorda slab and the Moho discontinuity are approximated from the compilation of geologic and geophysical data in the Coast Ranges [Page et al., 1998]. The basic parameter of our thermal model is the uniform initial temperature gradient $\sim 15^\circ\text{C}/\text{km}$, chosen to satisfy the observed heat flow values in northernmost California and southern Oregon (Figure 1). To the south of the MTJ (Figure 4b) we initially

Table 1. Rheological and Thermal Parameters Used in Modeling

Parameter	Meaning	Dimension	Crust	Mantle
ρ	Density	kg/m ³	2850	3300
K	Bulk modulus	GPa	63	122
G	Shear modulus	GPa	40	74
$\log B_N$	Dislocation creep constant	1/Pa ^{<i>n</i>} /s	-21.05	-16.3
H_N	Dislocation creep enthalpy	kJ/mol	445	535
n	Dislocation creep exponent	...	4.2	3.5
μ_0	Initial friction coefficient	...	0.6	0.6
c	Cohesion	MPa	20	20
α	Thermal expansivity	1/K	2.7×10^{-5}	3.0×10^{-5}
C_p	Specific heat	J/kg/K	1200	1200
λ	Thermal conductivity	W/m/K	2.5	3.3
A	Radiogenic heat production	W/kg	0.5×10^{-9}	0.0

assume a direct upwelling of the hot (1300°C) asthenospheric material to the depth 10 km below the top of the Gorda slab. In the 10 km transition zone we assign linear temperature distribution between the asthenospheric temperature and the temperature on the top of the slab. The following initial thicknesses of the tectonic elements are suggested: 40 km (20 Myr old) [Furlong, 1984] for the Pacific (Figure 4b) and Monterey (Figure 4c) plates, and 25 km for the Gorda slab (Figure 4a). Initial temperature within these tectonic elements is also assumed to change linearly with thickness (Figure 4).

[30] We neglect the along-strike variations of the crustal thickness in the initial crustal model. However, the thickness of the crustal layer is allowed to vary during the simulation. These variations are tracked by the finite element mesh. The upper and lower crustal layers are not differentiated by the mechanical properties. The material parameters used for the crust and the mantle are given in Table 1. Within the Salinian block we deactivate the strain softening to preclude generation of faults and allow it to move as a relatively rigid terrain.

3. Slab Window Cooling

[31] In the vicinity of MTJ the temperature distribution is unsteady due to large horizontal and vertical gradients. As the triple junction migrates northwestward the temperature gradients equilibrate by conductive cooling. This process is shown in Figure 6 (see also Animation S1 in the auxiliary material).¹ The equilibration causes eastward motion of the

locus of maximum mantle temperature and minimum viscosity. Since the lowest viscosity implies also the lowest strength (shear stress), the plate boundary should displace eastward, both in the mantle and in the crust. However, the effect of the slab window cooling is counteracted by the effects of shear heating in the mantle, step-induced transpression, and slip weakening on the faults. To study all these effects simultaneously we first consider a simplified model without microplate and crustal block. To put the accent on the temperature-related processes, we constrain the saturated slip-dependent friction on the faults to be 0.12 according to the best fit estimate of Bird and Kong [1994].

3.1. Effect of Shear Heating and Slip Weakening

[32] The heating processes related to the shear deformation can produce significant local perturbations in the temperature field. Hartz and Podladchikov [2008] showed that this mechanism can cause up to tenfold reduction of the effective strength of typical lithosphere. Substantial part of this reduction occurs due to viscous deformation in the mantle. In the cold brittle crust the viscosities are too high to be influenced by the shear heating. Therefore, the shear heating can significantly increase stability of the long-term persisting fault due to weakening of mantle roots. The drop of the effective friction coefficient related to the accumulated slip can intensify this effect. Both these mechanisms act like inhibitors of the plate boundary migration in the direction of the slab window thermal impulse.

[33] The results of our three-dimensional models confirm these considerations. We calculated a series of models with variable magnitude of shear heating efficiency parameter (χ in equation (2)),

¹Auxiliary materials are available in the HTML. doi:10.1029/2012GC004086.

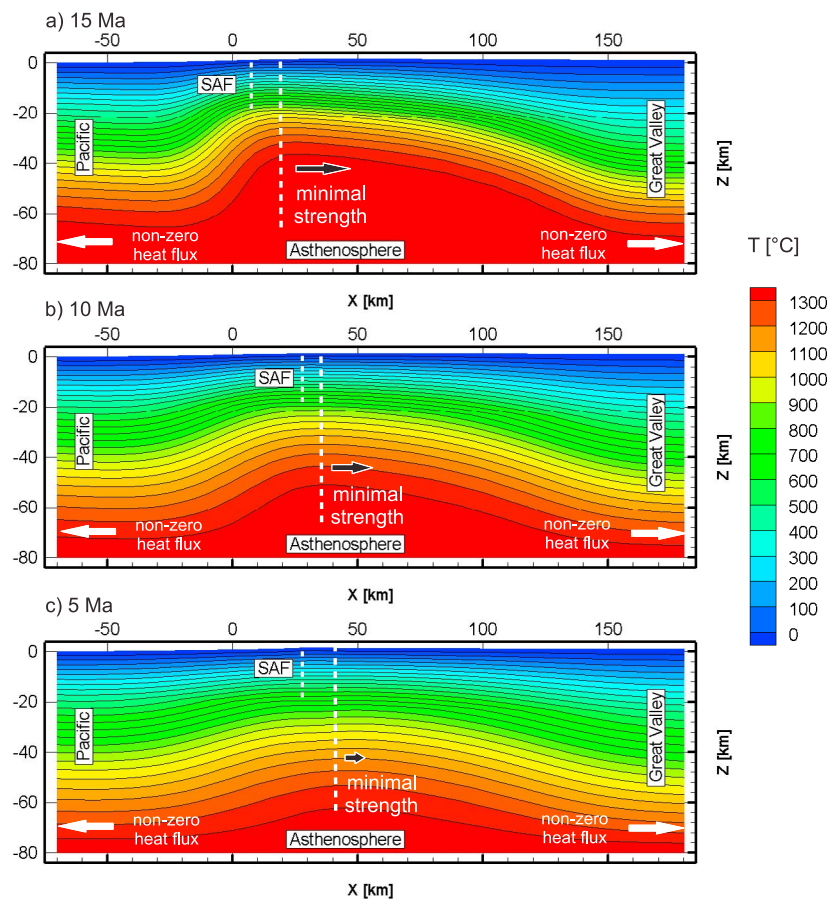


Figure 6. Slab window cooling and eastward migration of lithospheric strength. Colors show distribution of the temperature at (a) 15 Ma, (b) 10 Ma, and (c) 5 Ma. The locus of the inferred minimum integrated lithospheric strength is shown with a dashed vertical line. White arrows indicate the nonzero heat flux on the vertical boundaries of the model.

which is the part of dissipated mechanical energy converted into heat. Figure 7 shows how the temperature field and terrain pattern after 18 Myr of strike-slip motion are changing with reducing shear heating in our models. If the shear heating is activated to the full extent, the model fails to displace the crustal plate boundary during the entire 18 Myr (Figure 7a). Only if we switch shear heating efficiency parameter to unrealistically low 10% value, the model responds with intensification of the eastward fault migration. The variation of mantle temperature field is shown in the vertical profiles across the plate boundary in Figure 7. Significant mantle temperature anomaly is detected in the model with 100% shear heating (Figure 7a). Local temperature perturbation beneath the fault causes the viscosity decrease, according to equation (6), thus reducing the lithospheric strength and making the older fault more attractive locus for the plate boundary.

[34] Predictions of the physically realistic 100% efficiency scenario contradict the observations. The observed crustal plate boundary does displace inland, as opposed to the model (Figure 7a). The shear heating must be decreased to unrealistically low values (10% of the entire shear heating value) to initiate the terrain accretion (Figure 7b). We suggest, therefore, that slab window cooling alone is insufficient to displace the crustal plate boundary. These results remain valid if we include other less important weakening mechanisms (e.g., grain size reduction). More weakening will penalize fault migration even further.

3.2. Effect of Transpression

[35] The style of plate boundary migration caused by the slab window cooling is characterized by the occurrence of restraining fault bends. It happens because the more southern segments of the fault

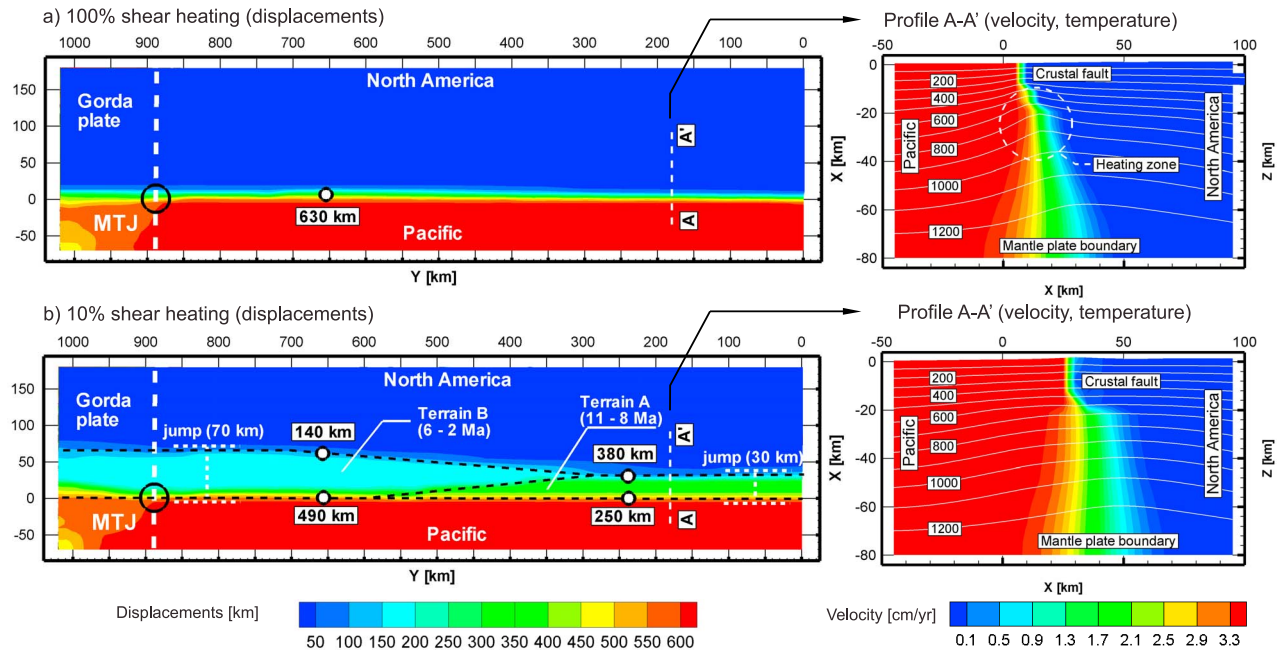


Figure 7. Influence of shear heating on the terrane accretion. The two different models with (a) 100% and (b) 10% shear heating efficiency (χ , equation (2)). Shown are the total strike-slip displacements (colors) on the top boundary of the model. Profiles show distribution of the strike-slip velocity (colors) and temperature (white lines). Note different meaning of color on the top views and in the profiles. Also shown are the accumulated slips on the faults (white circles with labels), terrane widths, and accretion time spans.

relating to the older and colder slab window parts tend to displace further inland, while the more northern segments locate closer to the ocean. In between these segments the strike-slip velocity vector is oriented obliquely to the fault, with significant fault-normal convergent component; i.e., transpression occurs. Accordingly, the fault “jumping” is inhibited, and can only occur if the driving force is larger than the tectonic force resulting from the transpression on the connecting fault segments. Figure 8 demonstrates the transpression zone formed after 30 km landward step of the southern fault segment (model with 50% shear heating). In the profile to the north of transpression zone (Figure 8b) there is large offset between the mantle and crustal plate boundaries with a sub-horizontal detachment zone. Within the transpression zone (Figure 8c) both the surface uplift and corresponding crustal thickening are detected.

4. Adding Microplate

[36] In this section we include a low-temperature perturbation in the southern part of the domain, which we interpret as the Monterey microplate lithosphere (Figures 3b and 4c). As the microplate

subduction is assumed to have been ceased, no low-friction subduction channel is placed between the Monterey and North American plates. We rule out the unrealistic low shear heating efficiency scenario and assume that the entire dissipated mechanical energy is converted into heat.

[37] The microplate, in general, create much stronger heterogeneity in the mantle than the cooling of the uprising asthenosphere. This factor dramatically decreases or even completely prohibits the generation of faults in the continent above the microplate. Hence, the plate boundary can instantly jump inland up to the microplate margins. This behavior is confirmed by the three-dimensional models presented here (Figure 9) (see also Animation S2). Initially, the plate boundary forms a large restraining bend which tends to bypass the microplate obstacle. In the northern and central parts of the domain the plate boundary locates near the western edge of the slab window. Further south it curves and strikes around the eastern margin of the microplate. The transpression resulting from this bend transmits the tectonic forces from the Pacific plate directly to the crustal blocks to the north of the microplate. Thus, the terrane accretion becomes

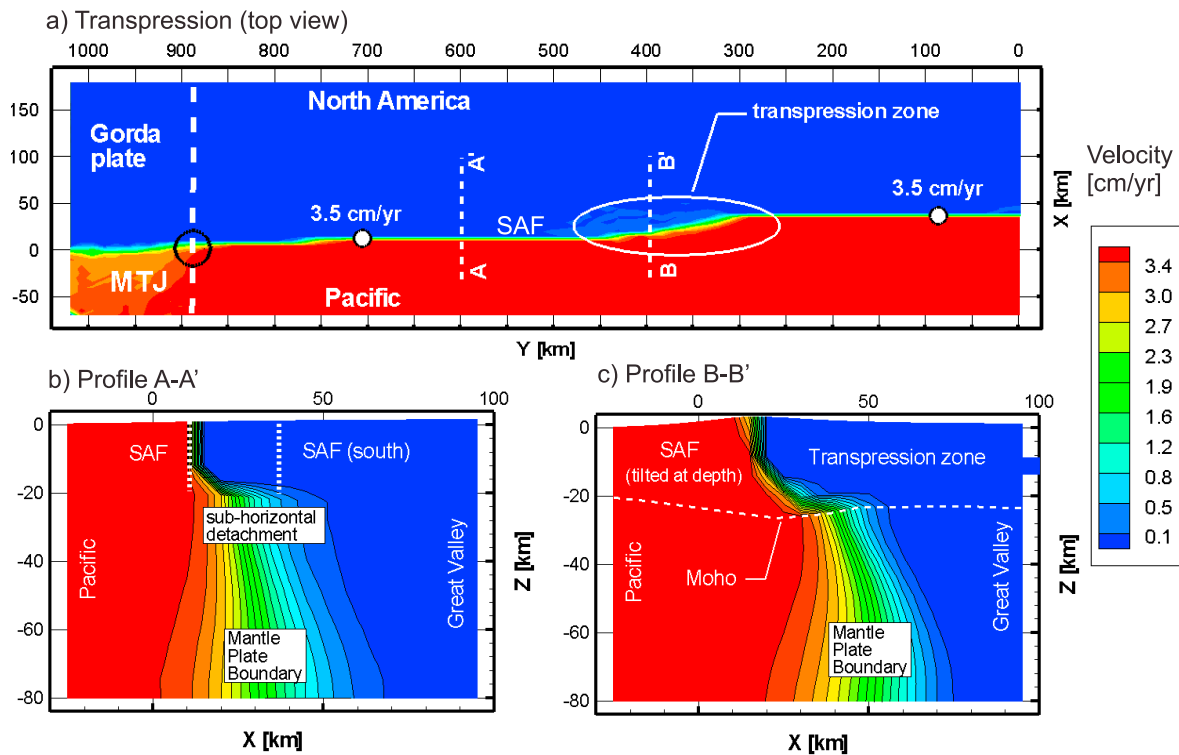


Figure 8. Influence of transpression on the terrane accretion. (a) The fault configuration in the model with 50% shear heating efficiency after the eastward (transpressive) fault step. Colors indicate the strike-slip velocities; white labeled circles are the slip rates on the major fault. (b and c) The profiles to the north (A-A') and across (B-B') the transpression zone, respectively.

greatly intensified by the microplate, compared to the slab window cooling scenario.

4.1. Effect of Fault Friction and “Strong” Crustal Block

[38] The magnitude of the saturated effective friction on the fault (see section 2.2 and Figure 5) has a twofold influence on the terrain accretion process in our models. Changing the saturated effective friction can simultaneously alter both the initiation of terrain capture and the rate of terrain velocity increase. With the best fit estimate of the San Andreas fault friction 0.12 of *Bird and Kong* [1994], the model predicts accretion of five distinct terranes marked as A–E in Figure 9a. Reducing the effective friction below this value systematically delays the terrane capture, and decreases the kinematic coupling between the terranes and Pacific plate.

[39] The style of terrain accretion is also influenced by the heterogeneities in the crust. To investigate this effect we calculated a simplified model with a crustal heterogeneity (Figures 3b and 4b), which we interpret as a Salinian block [Irwin, 1990]. According to the observations, the neighboring geological formations (Franciscan

assemblage and Great Valley sequence) are composed of the weaker strata than the plutonic rocks of Salinian block. In the model the higher strength of the block is achieved by deactivating the strain softening, such that the friction within the block remains equal to the initial value (0.6). The presented model is not aimed at explaining the origin or evolution of the Salinian block, but rather at studying its influence on the continental deformation.

[40] The presence of Salinian block significantly intensifies the rate of terrain transfer and degree of coupling. The new model identifies at maximum three terranes (Figure 9c): the southern unnamed terrane (A), the Salinian block (B), and the block located to the north (C), which we interpret as the San Francisco Bay Area block. In this work we constrain the effective friction on the faults by attempting to fit approximately the observed terrain pattern and magnitude of accumulated fault slip. For example, if the friction is reduced to very low value (0.06), the capture of Bay Area block does not occur until present time (Figure 9b). Our current best fit estimate (reference model) of the saturated fault friction is ~ 0.08 , which is comparable but slightly less than the value 0.12 obtained by

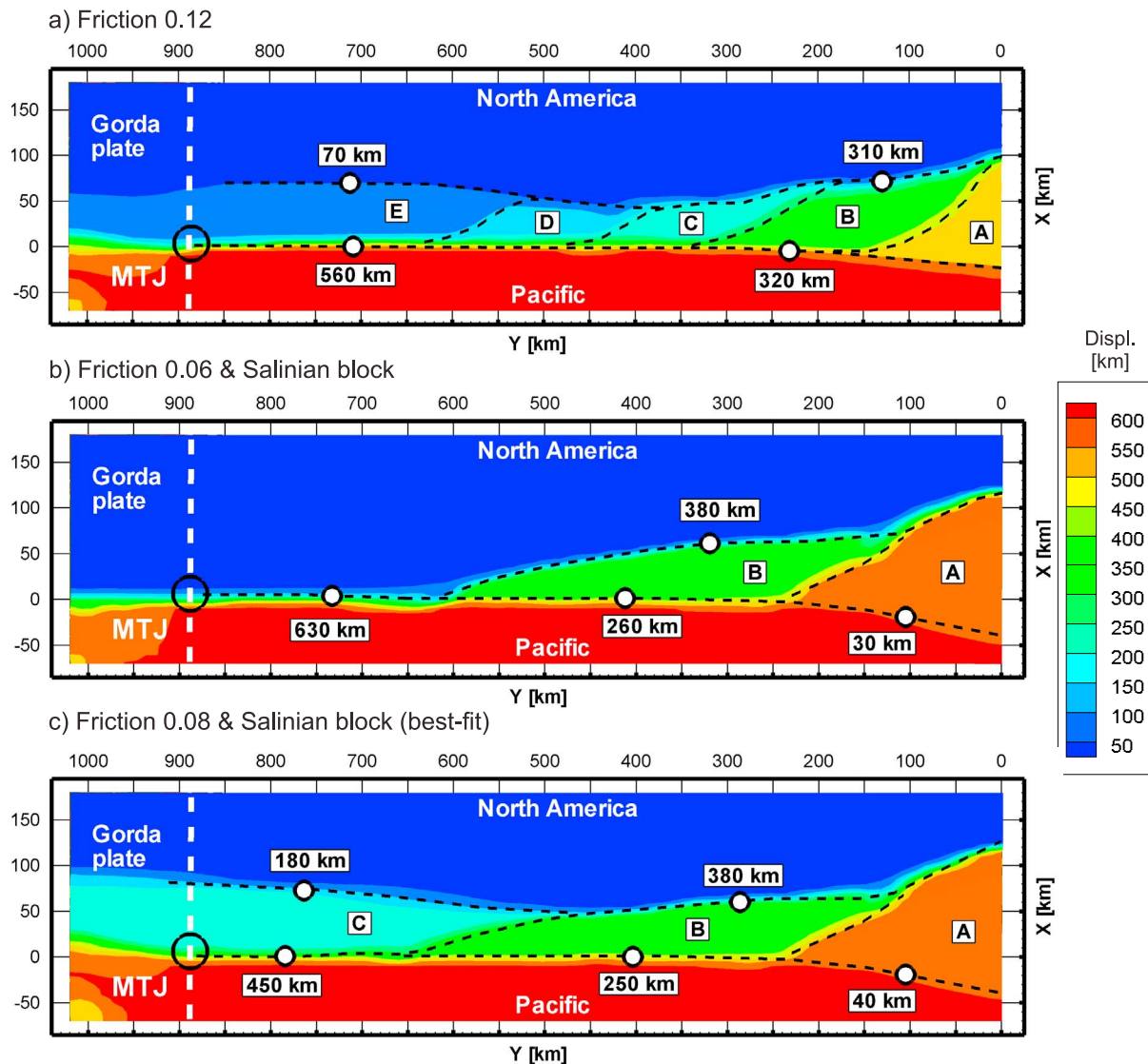


Figure 9. Influence of the microplate and strong crustal block on the terrane accretion. Shown are the total strike-slip displacements (colors) on the top boundary of the model. Distinct terranes are labeled with letters. White circles with labels indicate accumulated slips. The faults are marked with dashed lines. (a) Results of the model without crustal block and with the saturated fault friction 0.12 according to *Bird and Kong* [1994]. (b) Results of the model with crustal block and saturated friction 0.06. (c) Results of the model with crustal block and saturated friction 0.08 (reference model).

Bird and Kong [1994]. The terrain configuration corresponding to the reference model is shown in Figure 9c (see also Animation S2).

5. Discussion

[41] Based on comparison of modeling results with observations for SAFS (see below), we claim that despite a relatively simple idealization, our models are able to resolve first-order features of SAFS structure and evolution. However, in no case our

results should be treated as a complete description of the complex Neogene tectonic history of the SAFS, because still the models contain many simplifications (discussed below).

5.1. Model Assumptions and Limitations

[42] According to the tectonic reconstructions of *Atwater and Stock* [1998] the Pacific plate velocity has significantly changed its direction with respect to the stable North America at about 8 Ma. In this study we specify the velocity of the Pacific plate with

respect to the Great Valley block, which remains largely uncertain. The Gorda (previously Juan de Fuca) plate has interacted dynamically with the mantle and the surrounding plates. Its velocity has been changing since at least 6.5 Ma [Riddihough, 1984]. The plate has behaved nonrigidly and accommodated significant deformations [Chaytor *et al.*, 2004]. Here we assume that both plates were rigid during the entire modeling time, and did not change neither the direction nor the magnitude of the velocity with respect to the Great Valley block. With this assumption we neglect normal component of relative velocity compared to much larger tangential velocity component between the Pacific plate and the Great Valley block. Yang and Liu [2010] have shown that gravitational spreading in northern Basin and Range plays a role on long-term deformation of Pacific-North American plate boundary. The influence of this factor is also considered to be beyond the scope of this study.

[43] The actual impact of the microplates on the tectonic evolution of the North America western margin is more complicated compared to our models. In particular, the Arguello, Guadalupe and Magdalena microplates [Stock and Lee, 1994] can transfer higher tractions from the Pacific than the Monterey microplate alone. We have selected the Monterey microplate as the closest to the modeled region, and presumably the most important. We argue that our approach is sufficient to demonstrate the difference between the slab window cooling and the microplate capture mechanisms. Our models can be further improved by starting the SAFS evolution from the ridge-trench collision and considering the plate interaction from the fully dynamic viewpoint. Such a complicated approach is however beyond the scope of this work.

[44] There are also other limitations of our model, e.g., simplified and not well constrained initial temperature distribution in the lithosphere, prescribed kinematics of the Gorda plate etc. Nevertheless we argue, that the mechanical equilibrium in the system is correctly reproduced to the first order. To demonstrate that we compare some of the results, such as the heat flow, fault offsets, and lithospheric structure, against the available observations.

5.2. Comparison With Observations

5.2.1. Offsets on Major Faults

[45] The reference model demonstrates good correlation with the reconstructed fault offsets near the

San Francisco Bay Area (Figure 10). However, the model does not resolve certain faults. For example, the Hayward-Calaveras fault system is represented with single eastern fault. The western margin of Salinian block is also bounded with single fault, which we interpret here as San Gregorio fault. The Bay area and Salinian terrains accommodated ~ 180 km and ~ 380 km displacements, respectively, in the fixed Great Valley frame since 18 Ma (Figure 10b). This values correlate relatively well with the total 160 km for the Hayward-Calaveras system and 315 km for the Central San Andreas as shown in Figure 10a in Dickinson [1997]. The 250 km slip on the western bounding faults of the Salinian block predicted by the reference model is larger than the reconstructed 155 km slip on the San Gregorio fault. This discrepancy can be explained by existence of the offshore faults which accommodated slip before or simultaneously with the San Gregorio fault.

5.2.2. Weak Versus Strong Faults

[46] Using the fault offset constraint, we investigate also whether the “strong fault” hypothesis [Scholz, 2000a, 2000b] gives feasible results in the context of the long-term (>1 Myr) deformation with the thermomechanical coupling. We have calculated a setup similar to the reference model, but with saturated friction on the fault equal to ~ 0.5 (i.e., strong faults). Such a model, however, fails to generate the zones of strain localization and distinct crustal terrains. Instead of these, the model predicts a broad (60 km wide) zone of distributed shear deformation, which approximately follows the zone of the minimal lithospheric strength (Figure 10c). Our results, therefore, provide another independent constraint supporting the weak fault in a strong crust hypothesis [Zoback, 2000; Chéry *et al.*, 2001].

5.2.3. Heat Flow

[47] The presented models clearly show the manifestation of the asthenosphere upwelling in the slab window (Figure 11). On the surface heat flow map (Figure 11a) there are only minor thermal anomalies (<5 mWm⁻²) related to the shear heating on the San Andreas plate boundary. Despite 100% assumed shear heating efficiency, the associated heat flow increase is very small, due to small effective friction. Therefore, the presented models naturally overcome the “heat flow paradox” [Lachenbruch and Sass, 1988] and explain the absence of localized heat flow

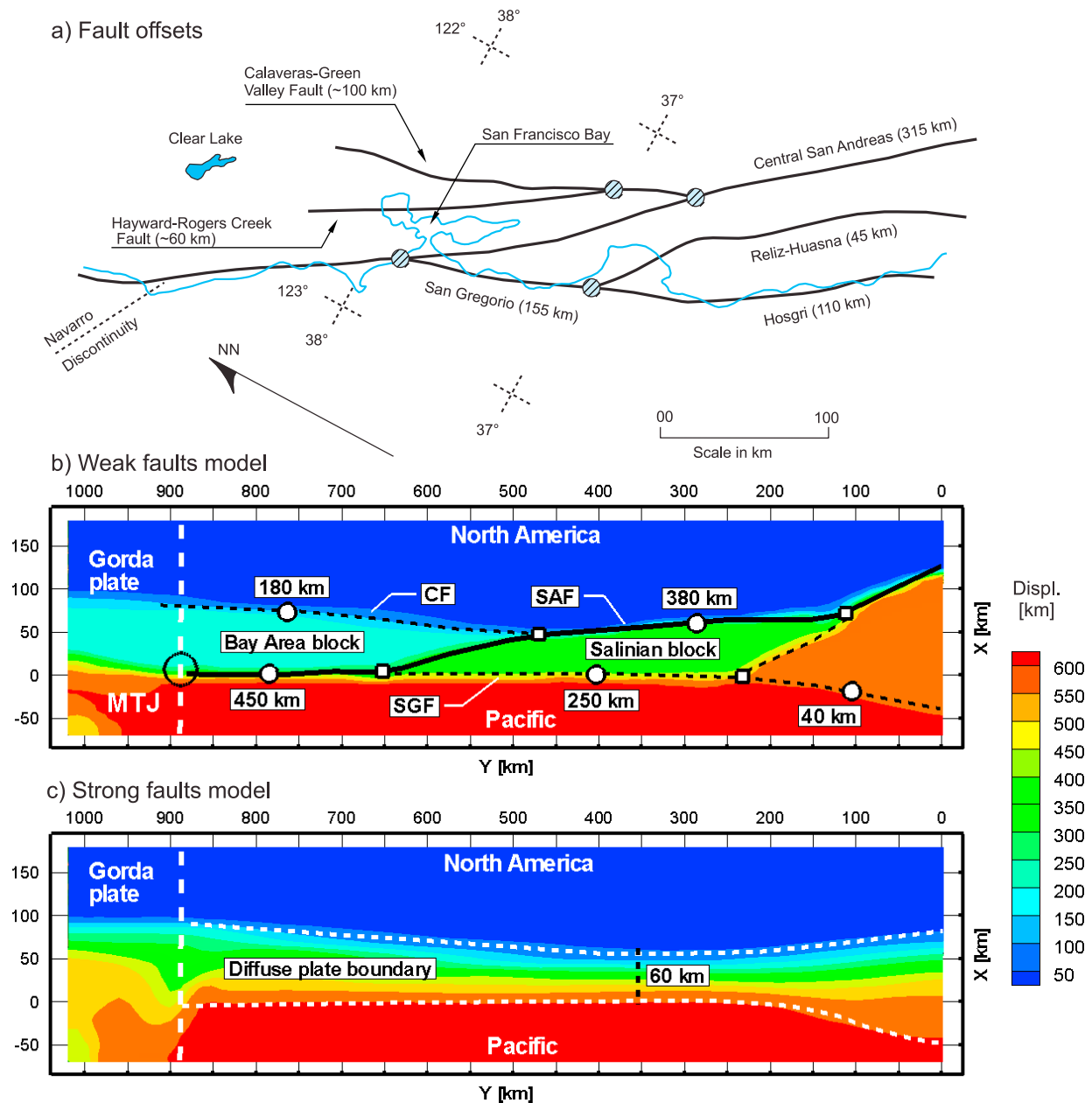


Figure 10. Interpretation of the terranes and faults in the reference model and comparison of the weak and strong fault models. Colors indicate strike-slip displacements. (a) Reconstructed fault offsets near the San Francisco Bay area (drawn after Dickinson [1997]). Thick lines mark faults; hatch circles define fault junctions. (b) Results of the reference model (weak faults). Fault offsets are displayed using the labeled white circles. White squares show fault junctions. Calaveras and Heyward faults are resolved in the model with one fault marked as CF (Calaveras Fault). The western faults including San Gregorio-Hosgri and Reliz-Huasna are represented by the fault marked as SGF (San Gregorio Fault). Two distinct terranes can be approximately identified as the Salinian and the Bay Area blocks. (c) Results of the model with the saturated friction ~ 0.5 (relatively strong faults). The model fails to form the distinct terranes and faults. The diffuse 60 km wide shear zone following the minimal lithospheric strength is predicted.

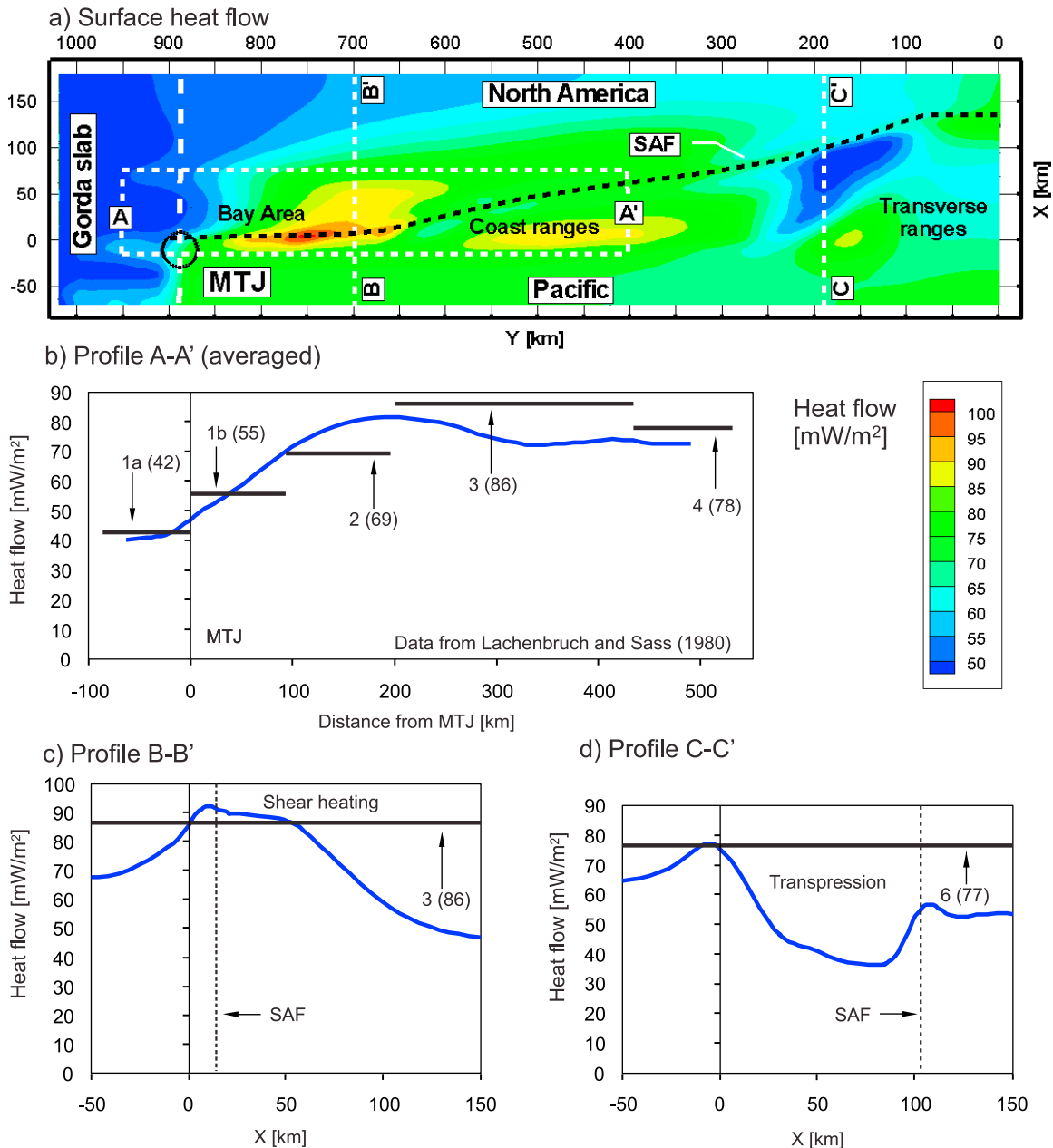


Figure 11. Comparison of the calculated and observed surface heat flow. (a) Surface heat flow map in the reference model. Colors indicate the heat flow magnitudes. Black dashed line show the trace of the interpreted San Andreas Fault. (b) Averaged heat flow along the strike-parallel profile A-A'. Averaging is performed over the width of rectangular area shown in Figure 11a. (c and d) The heat flow distribution along the strike-perpendicular profiles B-B' and C-C', respectively. Black horizontal bars show the averaged heat flow magnitudes for different regions along the San Andreas Fault [Lachenbruch and Sass, 1980].

anomaly without excessive hydrothermal activity. In general, the observed heat flow correlates with observations [Lachenbruch and Sass, 1980] relatively well, in both strike-parallel (Figure 11b) and strike-perpendicular profiles (Figure 11c). The averaged heat flow over the Coast Ranges initially

increases up to 83 mWm^{-2} at 200 km distance from the Mendocino triple uncton. Further south it decreases to the average value of 75 mWm^{-2} at 300 km distance. Figure 11d shows the prominent influence of the long-term transpression on the surface heat flow. In the southern part of the

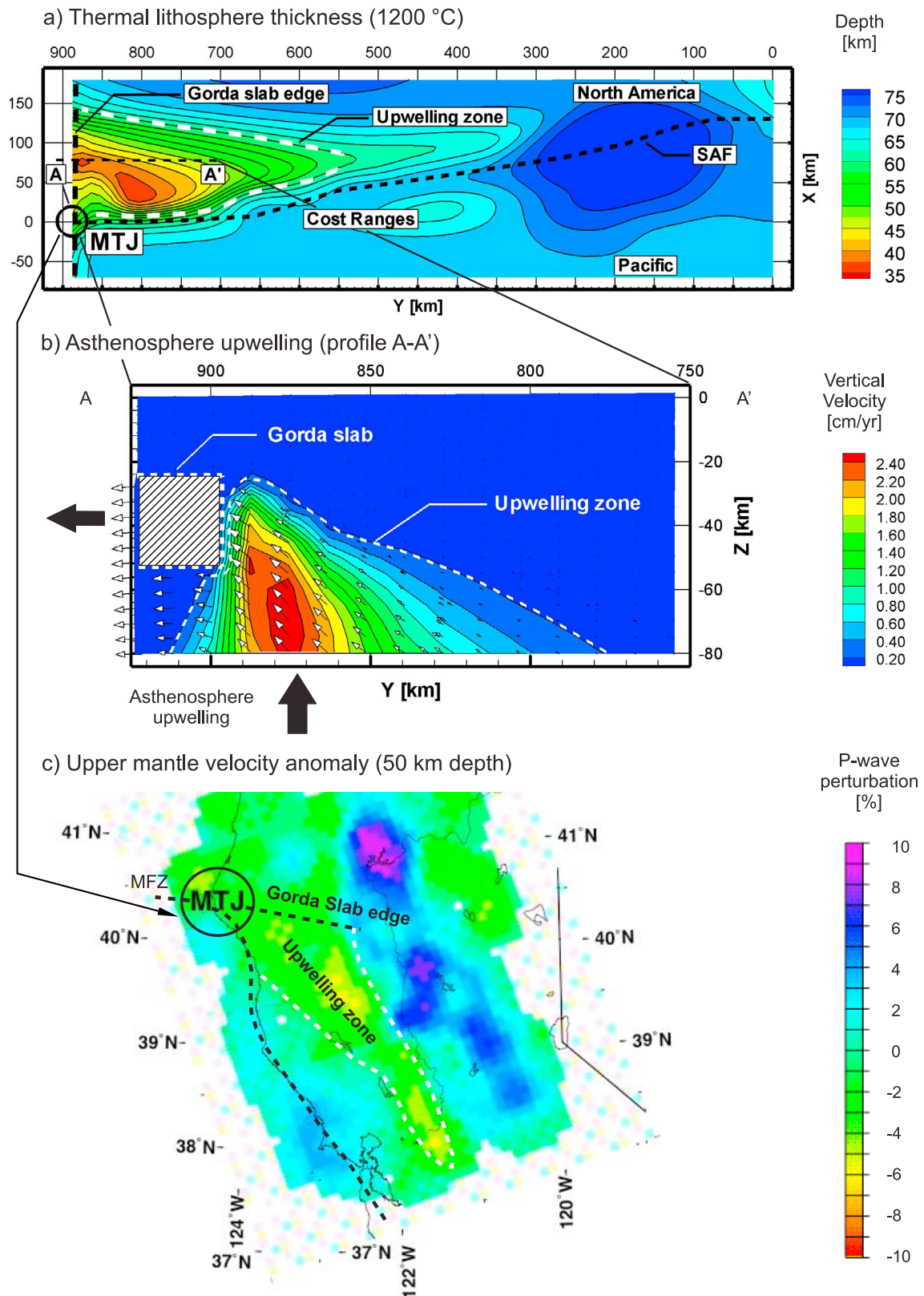


Figure 12

model near the restraining bend, the average heat flow value becomes locally overprinted by rapid crustal thickening.

5.2.4. Asthenosphere Upwelling

[48] The three-dimensional flow of the material in the slab window is a distinctive feature of the models presented in this work. The map of the thermal lithosphere thickness shows a relatively confined zone of active asthenosphere upwelling, with the center locating about 100 km to the south of MTJ (Figure 12a). This distance correlates with the current position of the upwelling center inferred from the fluid sources within the upper mantle [Levander *et al.*, 1998]. The predicted lithospheric thickness around the upwelling center is ~ 35 km. The upwelling zone inferred from the material velocities is even more confined than the zone of shallower thermal lithosphere (Figure 12b). Almost entire asthenosphere material enters the slab window within the first 50 km from the southern edge of Gorda slab. The discrepancy between the thermal and mechanical lithosphere can be explained by delays due to conductive cooling and gradual accretion of the asthenosphere to the overlying continent. Figure 12c shows the P wave velocity structure beneath northern California at 50 km depth [Benz *et al.*, 1992]. The low-velocity body beneath the Coast Ranges is interpreted as the zone of the high temperature and partial melting within the mantle caused by asthenosphere upwelling. In general, the size and shape of the shallow lithosphere zone in the reference model (Figure 12a) is comparable with the configuration of the low-velocity body beneath the Coast Ranges. The western edge of the upwelling zone coincides with the active mantle plate boundary in our models.

6. Conclusions

[49] Our study synthesizes two previously suggested geological concepts regarding the landward

propagation of the San Andreas plate boundary. Using a relatively simple finite element model we have shown that both the captured microplate and the slab window cooling can have a prominent impact on the Neogene deformation of the overlying North American plate. The models, however, reveal that driving force resulting from the slab window thermal equilibration is insufficient to overcome the compound effect of the shear heating of the mantle roots beneath faults, slip weakening, and step-induced transpression on the fault. On the other hand, the stalled microplates in the fossil Farallon subduction zone (e.g., Monterey microplate) can cause much larger strength heterogeneities in the mantle, than slow cooling of the slab window. Thus, the accretion of the North American terrains toward the Pacific plate becomes greatly intensified by presence of the microplates. From our results we, therefore, conclude that the microplate capture is probably the most important mechanism responsible for evolution of the SAFS.

[50] Similar to many previous numerical models of SAFS we conclude that the effective friction on the mature fault must be much lower than in the surrounding crust. The best fit model implies friction coefficient at mature faults of 0.08, about one order lower than dry friction for common rocks. The new aspect of our conclusion is that it is based not at present day fault dynamics, stress field or thermal structure, as in previous studies but on analyses of a long-term (20 Myr) evolution of SAFS.

Acknowledgments

[51] This work was funded by German Research Foundation (DFG grant So 425/2) and German Research Centre for Geosciences (GFZ Potsdam). A.P. was also partially funded by the European Research Council under the European Community's Seventh Framework program (FP7/2007-2013), ERC Grant agreement 258830. This support is gratefully acknowledged. A.P. wishes to thank Gary S. Fuis for helpful discussions regarding the microplate capture model. This manuscript benefited from constructive comments of two anonymous reviewers.

Figure 12. Comparison of the asthenosphere upwelling predicted by the reference model and interpreted from the P wave seismic tomography. (a) Thermal lithosphere thickness. Colors indicate the distance between the top boundary and the 1200°C isosurface in km. White dashed lines show the approximate extents of the active upwelling zone. (b) Distribution of vertical velocities in the upwelling zone from the reference model (profile A-A'). Colors show the magnitudes of the vertical velocities. Vectors indicate the material flow in the upwelling zone behind the Gorda slab (hatched area). (c) P wave seismic tomography of northern California upper mantle at 50 km depth [Benz *et al.*, 1992]. Colors indicate P wave velocity perturbations. Positive velocity anomaly is interpreted as the asthenospheric upwelling in the slab window.

References

- Argus, D. F., and R. G. Gordon (2001), Present tectonic motion across the Coast Ranges and San Andreas Fault system in central California, *Geol. Soc. Am. Bull.*, *113*, 1580–1592.
- Atwater, T. (1970), Implications of plate tectonics for the Cenozoic tectonic evolution of western North America, *Geol. Soc. Am. Bull.*, *81*, 3513–3536.
- Atwater, T., and P. Molnar (1973), Relative motions of the Pacific and North American plates deduced from seafloor spreading in the Atlantic, Indian, and South Pacific Oceans, in *Proceedings of the Conference on Tectonic Problems of the San Andreas Fault System*, edited by R. L. Kovach and A. Nur, *Stanford Univ. Publ. Geol. Sci.*, *13*, 136–148.
- Atwater, T., and J. Stock (1998), Pacific-North America plate tectonics of the Neogene southwestern United States: An update, *Int. Geol. Rev.*, *40*, 375–402.
- Beaudoin, B. C., et al. (1996), Transition from slab to slabless: Results from the 1993 Mendocino triple junction seismic experiment, *Geology*, *24*, 195–199.
- Becker, T. W., J. L. Hardebeck, and G. Anderson (2005), Constraints on fault slip rates of the Southern California plate boundary from GPS velocity and stress inversions, *Geophys. J. Int.*, *160*, 634–650.
- Benz, H. M., G. Zandt, and D. H. Oppenheimer (1992), Lithospheric structure of northern California from teleseismic images of the upper mantle, *J. Geophys. Res.*, *97*, 4791–4807.
- Bird, P., and X. Kong (1994), Computer simulations of California tectonics confirm very low strength of major faults, *Geol. Soc. Am. Bull.*, *106*, 159–174.
- Bohannon, R. G., and T. Parsons (1995), Tectonic implications of post-30 Ma Pacific and North American relative plate motions, *Geol. Soc. Am. Bull.*, *107*, 937–959.
- Burkett, E. R., and M. I. Billen (2009), Dynamics and implications of slab detachment due to ridge-trench collision, *J. Geophys. Res.*, *114*, B12402, doi:10.1029/2009JB006402.
- Byerlee, J. (1978), Friction of rocks, *Pure Appl. Geophys.*, *116*, 615–629.
- Carena, S., and C. Moder (2009), The strength of faults in the crust in the western United States, *Earth Planet. Sci. Lett.*, *287*, 373–384.
- Chaytor, J. D., C. Goldfinger, R. P. Dziak, and C. G. Fox (2004), Active deformation of the Gorda plate: Constraining deformation models with new geophysical data, *Geology*, *32*, 353–356.
- Chéry, J., M. D. Zoback, and R. Hassani (2001), An integrated mechanical model of the San Andreas Fault in central and northern California, *J. Geophys. Res.*, *106*, 22,051–22,066.
- Dickinson, W. R. (1981), Plate tectonics and the continental margin of California, in *The Geotectonic Development of California, Rubey*, vol. 1, edited by W. G. Ernst, pp. 1–28, Prentice Hall, Englewood Cliffs, NJ.
- Dickinson, W. R. (1997), Tectonic implications of Cenozoic volcanism in coastal California, *Geol. Soc. Am. Bull.*, *109*, 936–954.
- Dickinson, W. R., and W. S. Snyder (1979), Geometry of subducted slabs related to San Andreas transform, *J. Geol.*, *87*, 609–627.
- Dickinson, W. R., M. Duca, L. I. Rosenberg, H. G. Greene, S. A. Graham, J. C. Clark, G. E. Weber, S. Kidder, W. G. Ernst, and E. E. Brabb (2005), Net dextral slip, Neogene San Gregorio-Hosgri fault zone, coastal California: Geologic evidence and tectonic implications, *Spec. Pap. Geol. Soc. Am.*, *391*, 1–43, doi:10.1130/2005.2391-4.1.
- Faulkner, D. R., and E. H. Rutter (2001), Can the maintenance of overpressured fluids in large strike-slip fault zones explain their apparent weakness?, *Geology*, *29*, 503–506.
- Fuchs, K., and B. Müller (2001), World stress map of the Earth: A key to tectonic processes and technological applications, *Naturwissenschaften*, *88*, 357–371.
- Furlong, K. P. (1984), Lithospheric behavior with triple junction migration: An example based on the Mendocino triple junction, *Phys. Earth Planet. Inter.*, *36*, 213–223.
- Furlong, K. P. (1993), Thermal-rheologic evolution of the upper mantle and the development of the San Andreas Fault system, *Tectonophysics*, *223*, 149–164.
- Furlong, K. P., and R. Govers (1999), Ephemeral crustal thickening at a triple junction: The Mendocino crustal conveyor, *Geology*, *27*, 127–130.
- Furlong, K. P., and S. Y. Schwartz (2004), Influence of the Mendocino triple junction on the tectonics of coastal California, *Annu. Rev. Earth Planet. Sci.*, *32*, 403–433.
- Furlong, K. P., W. D. Hugo, and G. Zandt (1989), Geometry and evolution of the San Andreas Fault zone in northern California, *J. Geophys. Res.*, *94*, 3100–3110.
- Gerya, T. (2010), Dynamical instability produces transform faults at mid-ocean ridges, *Science*, *329*, 1047–1050.
- Groome W. G., and D. J. Thorkelson (2009), The three-dimensional thermo-mechanical signature of ridge subduction and slab window migration, *Tectonophysics*, *464*, 70–83.
- Harlow, F. H., and J. E. Welch (1965), Numerical calculation of time-dependant viscous incompressible flow of fluid with free surface, *Phys. Fluids*, *8*, 2182–2189.
- Hartz, E. H., and Y. Y. Podladchikov (2008), Toasting the jelly sandwich: The effect of shear heating on lithospheric geotherms and strength, *Geology*, *36*, 331–334.
- Hickman, S., and M. Zoback (2004), Stress orientations and magnitudes in the SAFOD pilot hole, *Geophys. Res. Lett.*, *31*, L15S12, doi:10.1029/2004GL020043.
- Humphreys, E. D., and D. D. Coblenz (2007), North American dynamics and western U.S. tectonics, *Rev. Geophys.*, *45*, RG3001, doi:10.1029/2005RG000181.
- Humphreys, E. D., and K. G. Dueker (1994), Western U.S. upper mantle structure, *J. Geophys. Res.*, *99*, 9615–9634.
- Ingersoll, R. V. (1982), Triple-junction instability as cause for late Cenozoic extension and fragmentation of the western United States, *Geology*, *10*, 621–624.
- Irwin, W. P. (1990), Geology and plate-tectonic development, in *The San Andreas Fault System, California*, edited by R. E. Wallace, *U.S. Geol. Surv. Prof. Pap.*, *1515*, 61–80.
- Kameyama, M., D. A. Yuen, and S.-I. Karato (1999), Thermal-mechanical effects of low-temperature plasticity (the Peierls mechanism) on the deformation of a viscoelastic shear zone, *Earth Planet. Sci. Lett.*, *168*, 159–172.
- Lachenbruch, A. H., and J. H. Sass (1980), Heat flow and energetics of the San Andreas Fault zone, *J. Geophys. Res.*, *85*, 6185–6222.
- Lachenbruch, A. H., and J. H. Sass (1988), The stress heat-flow paradox and thermal results from Cajon Pass, *Geophys. Res. Lett.*, *15*, 981–984.
- Lachenbruch, A. H., and J. H. Sass (1992), Heat flow from Cajon Pass, fault strength, and tectonic implications, *J. Geophys. Res.*, *97*, 4995–5015.
- Levander, A., T. J. Henstock, A. S. Meltzer, B. C. Beaudoin, A. M. Trehu, and S. L. Klemperer (1998), Fluids in the lower crust following Mendocino triple junction migration: Active basaltic intrusion?, *Geology*, *26*, 171–174.

- Li, Q., M. Liu, and H. Zhang (2009), A 3-D viscoelastoplastic model for simulating long-term slip on non-planar faults, *Geophys. J. Int.*, *176*, 293–306.
- Liu, M., Y. Yang, Q. Li, and H. Zhang (2007), Parallel computing of multi-scale continental deformation in the Western United States: Preliminary results, *Phys. Earth Planet. Inter.*, *163*, 35–51.
- Liu, M., H. Wang, and Q. Li (2010), Inception of the eastern California shear zone and evolution of the Pacific-North American plate boundary: From kinematics to geodynamics, *J. Geophys. Res.*, *115*, B07401, doi:10.1029/2009JB007055.
- Liu, Z., and P. Bird (2002), North America plate is driven westward by lower mantle flow, *Geophys. Res. Lett.*, *29*(23), 2164, doi:10.1029/2002GL016002.
- Lonsdale, P. (1991), Structural patterns of the Pacific floor offshore of peninsular California, in *The Gulf and Peninsula Province of the Californias*, edited by J. P. Dauphin and B. T. Simoneit, *AAPG Mem.*, *47*, 87–125.
- Morrow, C. A., D. E. Moore, and D. A. Lockner (2000), The effect of mineral bond strength and absorbed water on fault gouge frictional strength, *Geophys. Res. Lett.*, *27*, 815–818.
- Nicholson, C., C. C. Sorlien, T. Atwater, J. C. Crowell, and B. P. Luyendyk (1994), Microplate capture, rotation of the western Transverse Ranges, and initiation of the San Andreas transform as a low-angle fault system, *Geology*, *22*, 491–495.
- Page, B. M., R. G. Coleman, and G. A. Thompson (1998), Late Cenozoic tectonics of the central and southern Coast Ranges of California, *Geol. Soc. Am. Bull.*, *110*, 846–876.
- Petrinin, A., and S. V. Sobolev (2006), What controls thickness of sediments and lithospheric deformation at a pull-apart basin?, *Geology*, *34*, 389–392.
- Petrinin, A. G., and S. V. Sobolev (2008), Three-dimensional numerical models of the evolution of pull-apart basins, *Phys. Earth Planet. Inter.*, *171*, 387–399.
- Popov, A. A., and S. V. Sobolev (2008), SLIM3D: A tool for three-dimensional thermomechanical modeling of lithospheric deformation with elasto-visco-plastic rheology, *Phys. Earth Planet. Inter.*, *171*, 55–75.
- Prescott, W. H., J. C. Savage, J. L. Svarc, and D. Manaker (2001), Deformation across the Pacific-North America plate boundary near San Francisco, California, *J. Geophys. Res.*, *106*, 6673–6682.
- Provost, A.-S., and H. Houston (2003), Stress orientations in northern and central California: Evidence for the evolution of frictional strength along the San Andreas plate boundary system, *J. Geophys. Res.*, *108*(B3), 2175, doi:10.1029/2001JB001123.
- Riddihough, R. (1984), Recent movements of the Juan de Fuca plate system, *J. Geophys. Res.*, *89*, 6980–6994.
- Scholz, C. H. (2000a), A fault in the ‘weak San Andreas’ theory, *Nature*, *406*, 234.
- Scholz, C. H. (2000b), Evidence for a strong San Andreas fault, *Geology*, *28*, 163–166.
- Severinghaus, J., and T. Atwater (1990), Cenozoic geometry and thermal state of the subducting lithosphere beneath North America, in *Basin and Range Extensional Tectonics Near the Latitude of Las Vegas, Nevada*, edited by B. P. Wernicke, *Mem. Geol. Soc. Am.*, *176*, 1–22.
- Simo, J. C., and T. J. R. Hughes (2000), *Computational Inelasticity*, *Interdisciplinary Appl. Math.*, vol. 7, 2nd ed., Springer, New York.
- Sobolev, S. V., and A. Y. Babeyko (2005), What drives orogeny in the Andes?, *Geology*, *33*, 617–620.
- Sobolev, S. V., A. Petrunin, Z. Garfunkel, A. Y. Babeyko, and DESERT Group (2005), Thermo-mechanical model of the Dead Sea transform, *Earth Planet. Sci. Lett.*, *238*, 78–95.
- Stock, J. M., and J. Lee (1994), Do microplates in subduction zones leave a geological record?, *Tectonics*, *13*, 1472–1487.
- Townend, J., and M. D. Zoback (2001), Implications of earthquake focal mechanisms for the frictional strength of the San Andreas Fault system, in *The Nature and Tectonic Significance of Fault Zone Weakening*, edited by R. E. Holdsworth et al., *Geol. Soc. Spec. Publ.*, *186*, 13–21.
- Townend, J., and M. D. Zoback (2004), Regional tectonic stress near the San Andreas Fault in central and Southern California, *Geophys. Res. Lett.*, *31*, L15S11, doi:10.1029/2003GL018918.
- van Wijk, J. W., R. Govers, and K. P. Furlong (2001), Three-dimensional thermal modeling of the California upper mantle: A slab window vs. stalled slab, *Earth Planet. Sci. Lett.*, *186*, 175–186.
- Wilson, D. S., P. A. McCrory, and R. G. Stanley (2005), Implications of volcanism in coastal California for the Neogene deformation history of western North America, *Tectonics*, *24*, TC3008, doi:10.1029/2003TC001621.
- Yang, Y., and M. Liu (2010), What drives short- and long-term crustal deformation in the southwestern United States?, *Geophys. Res. Lett.*, *37*, L04306, doi:10.1029/2009GL041598.
- Zandt, G., and K. P. Furlong (1982), Evolution and thickness of the lithosphere beneath coastal California, *Geology*, *10*, 376–381.
- Zienkiewicz, O. C., and R. L. Taylor (2000), *The Finite Element Method*, 5th ed., Butterworth-Heinemann, Oxford, U. K.
- Zoback, M. D. (2000) Strength of the San Andreas, *Nature*, *405*, 31–32.
- Zoback, M. D. (2007), *Reservoir Geomechanics*, Cambridge Univ. Press, Cambridge, U. K.
- Zoback, M. D., and J. H. Healy (1992), In situ stress measurements to 3.5 km depth in the Cajon Pass scientific research borehole: Implications for the mechanics of crustal faulting, *J. Geophys. Res.*, *97*, 5039–5057.
- Zoback, M. D., et al. (1987), New evidence on the state of stress of the San Andreas Fault system, *Science*, *238*, 1105–1111.